EMBRY-RIDDLE
Aeronautical University™
SCHOLARLY COMMONS

Fall 1996

Detection of Fatigue Crack Growth in a Simulated Aircraft Fuselage

Michael Lee Marsden
Embry-Riddle Aeronautical University - Daytona Beach

Follow this and additional works at: https://commons.erau.edu/db-theses

Part of the Aerospace Engineering Commons, and the Aviation Commons

Scholarly Commons Citation

DETECTION OF FATIGUE CRACK GROWTH IN A

SIMULATED AIRCRAFT FUSELAGE

by

Michael Lee Marsden

A Thesis Submitted to the Graduate Studies Office
in Partial Fulfillment of the Requirements for the Degree of
Master of Science in Aerospace Engineering

Embry-Riddle Aeronautical University
Daytona Beach, Florida
Fall 1996

UMI Number: EP31949

INFORMATION TO USERS

The quality of this reproduction is dependent upon the quality of the copy submitted. Broken or indistinct print, colored or poor quality illustrations and photographs, print bleed-through, substandard margins, and improper alignment can adversely affect reproduction.

In the unlikely event that the author did not send a complete manuscript and there are missing pages, these will be noted. Also, if unauthorized copyright material had to be removed, a note will indicate the deletion.
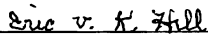
UMI®

DETECTING FATIGUE CRACK GROWTH IN A

SIMULATED AIRCRAFT FUSELAGE

by
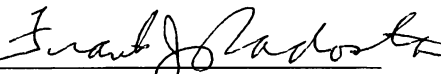
Michael Lee Marsden

This thesis was prepared under the direction of the candidate's thesis committee chairman, Dr. Eric v. K. Hill, Department of Aerospace Engineering, and has been approved by the members of his thesis committee. It was submitted to the Department of Aerospace Engineering and was accepted in partial fulfillment of the requirements for the degree of Master of Science in Aerospace Engineering

THESIS COMMITTEE

Dr. Eric v. K. Hill
Chairman

Dr. Frank J. Radosta
Member

Mr. Christopher J. Raczkowski
Member

Coordinator, MSAE

Department Chair, Aerospace Engineering

12/13/96
Date

ACKNOWLEDGMENTS
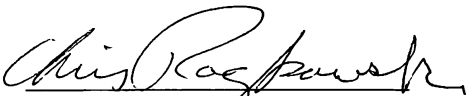
ABSTRACT

Author: Michael Lee Marsden

Title: Detecting Fatigue Crack Growth in a Simulated Aircraft Fuselage

Institution: Embry-Riddle Aeronautical University

Degree: Master of Science in Aerospace Engineering

Year: 1996

Acoustic emission (AE) nondestructive testing can detect fatigue cracks as they occur in complex structures. One use for AE has been in-flight detection of fatigue cracks in aircraft. The KC-135 aircraft were successfully monitored as early as 1979. The main problem with this and subsequent applications was an unfavorable signal to noise ratio, the key being to separate the small amplitude crack signals from the large amplitude ambient noise. This was accomplished here through the use of a Kohonen self-organizing map (SOM) neural network.

In order to simulate a fuselage undergoing fatigue, a pressure vessel was constructed from a 0.040 inch thick 2024-T3 aluminum cylinder. The vessel contained a rivet line, a round hole with a notch filed in it to provide a stress concentration, and a repair patch and was cyclically pressurized from 20 to 80 psi in order to fatigue the aluminum and generate typical in-flight signals. During the test, AE sensors, powered by a data acquisition system, collected the AE parameter data from metal rubbing at the patch, rivet fretting at the rivet line, and fatigue crack propagation at the stress concentration. The SOM successfully separated the crack signals from the rivet and rubbing signals. A prototype system is currently being built by Martingale Research Corporation to provide aircraft with a real time in-flight fatigue crack growth monitoring capability.

TABLE OF CONTENTS

Page

LIST OF FIGURES AND TABLES

CHAPTER 1

INTRODUCTION

1.1 OVERVIEW

As aircraft exceed their design lives, the number of aging aircraft is steadily increasing. A major problem for these aging aircraft is fatigue cracking. Catastrophic fatigue crack growth was the cause of the April, 1988 Aloha Airlines 737-200 incident where a large section of the upper fuselage ripped off shortly after takeoff [O'Lone]. The number of such incidents will doubtless continue to rise until a viable system is in place to detect fatigue crack growth while it is occurring. Such a system could be built using acoustic emission (AE) nondestructive testing to detect stable fatigue crack growth coupled with a neural network to sort out fatigue crack growth signals from the many other noises present.

Airlines have partially side-stepped the aging aircraft problem by implementing scheduled inspections and a parts replacement system. This solution avoids having to purchase brand new aircraft (the best but most expensive alternative) but does not solve the problem completely: it only delays it. As the aging fleet increases in size, the parts replacement system will quite possibly become bogged down with the large number of replacements needed. To save time and money, the airlines need a monitoring system to warn maintenance personnel when a part needs replacement due to wear and not for time in service.

1.2 PREVIOUS RESEARCH

Several attempts have been made to monitor aircraft in flight for fatigue crack propagation. These include the C/KC-135 [Parrish], the Avro CF-100 [McBride and Maclachlan], the French Mirage [Scala and Coyle], the F-15 [*Materials Evaluation*], and the F/A-18 [Scala, McCardle, and Bowles]. Each of these aircraft employed AE instrumentation to detect failures in either the fuselage, bulkhead, or wing attachment points -- fatigue-critical parts. In every case, the fact that aircraft are structurally very noisy made classification of the failure mechanisms a tedious process, at best. None of these systems employed a neural network to sort out the various failure mechanisms present.

Some recent work has been done to classify AE source waveforms using neural networks. Classification neural networks called self-organizing maps (SOMs) have been used to sort out rivet fretting and crack propagation in riveted double lap joints [Almeida] and the failure mechanisms in composite tensile test specimens such as matrix cracking, fiber breakage, and delaminations [Ely]. A SOM was also used to classify failure mechanisms from the frequency spectra of the signals emanating from a thin aluminum pressure vessel during cyclic loading [Thornton].

1.3 CURRENT APPROACH

The purpose of this research is to apply neural networks to classical AE parameter data in order to identify stable fatigue crack propagation signals in a thin aluminum pressure vessel (utilized to simulate an aircraft fuselage) undergoing cyclic pressurization fatigue. Resonant AE sensors are used to monitor the stress wave activity in the pressure vessel. The sensors transmit an electrical signal to the data acquisition system which extracts the six AE

quantification parameters (amplitude, counts, duration, risetime, energy, and counts-to-peak) from the signals. These AE parameter data are used to train a series of SOMs. Other AE parameter data sets are then used to test these SOMs. The trained SOMs group similar parameter sets into clusters. These clusters represent the AE sources present in the vessel.

This approach differs from the previous research [Thornton] primarily in the type of data collected. The previous research collected raw waveforms from the pressure vessel with a wideband AE sensor. The power spectrum of each waveform was found and broken down into 67 equal parts. These were used as inputs to a series of SOM neural networks. The output was a two-dimensional topographical map containing clusters which represented the failure mechanisms in the vessel. It is believed that the current approach is an improvement over Thornton's work primarily due to the greater precision in classifying the failure mechanisms present in the vessel, but also due to the decrease in data processing required.

CHAPTER 2

BACKGROUND THEORY

2.1 ACOUSTIC EMISSION

2.1.1 PHENOMENOLOGY

Acoustic emission nondestructive testing can be used to detect failure in loaded

structures. Some other uses of AE are leak testing, crack detection, tool wear assessment,

and weld monitoring [Miller and McIntyre]. Acoustic emission has many advantages over

other NDT techniques. The greatest of these may be the global monitoring capability of AE.

Because of its extreme sensitivity, AE can be used to passively monitor an entire structure

with a few sensors. Techniques such as eddy current, radiography, and ultrasonics can only

monitor a small portion of the structure at one time. Another advantage that AE has over

other NDT techniques is that the part being tested does not have to be removed from the

surrounding structure. In fact, the part is oftentimes monitored while in service. These two

advantages -- global and in-service monitoring -- make AE a viable candidate for in-flight

fatigue crack detection.

Acoustic emission sensors, as shown in Figures 2.1 and 2.2, detect stress waves

propagating through the material. These waves are generated by a rapid release of energy,

such as that associated with fatigue crack growth. The piezoelectric element in the sensor

emits a voltage in response to the energy input. In Figure 2.1, the couplant layer acts as a

waveguide for the energy waves in the material to be sensed by the AE transducer. Figure 2.2

depicts an AE transducer sensing the energy from a propagating crack in a specimen and

sending an electrical signal to the data acquisition system.

The electrical signal, which represents a stress wave in the material, is sent to the AE

data acquisition system. It amplifies the signal, then performs a feature extraction to

determine values of the AE quantification parameters for each signal. These AE parameters

are amplitude, counts, duration, energy, risetime, and counts-to-peak.
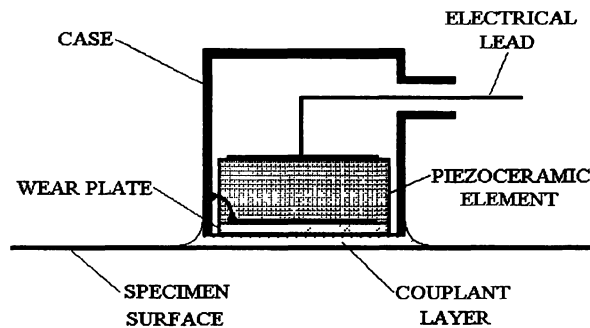
Figure 2.1 Acoustic Emission Sensor
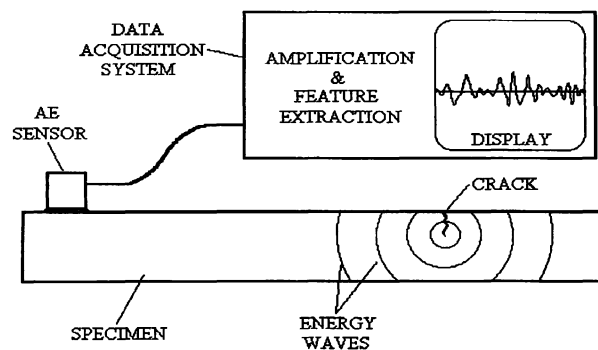
Figure 2.2 AE Sensor Sending a Signal to the Data Acquisition System.
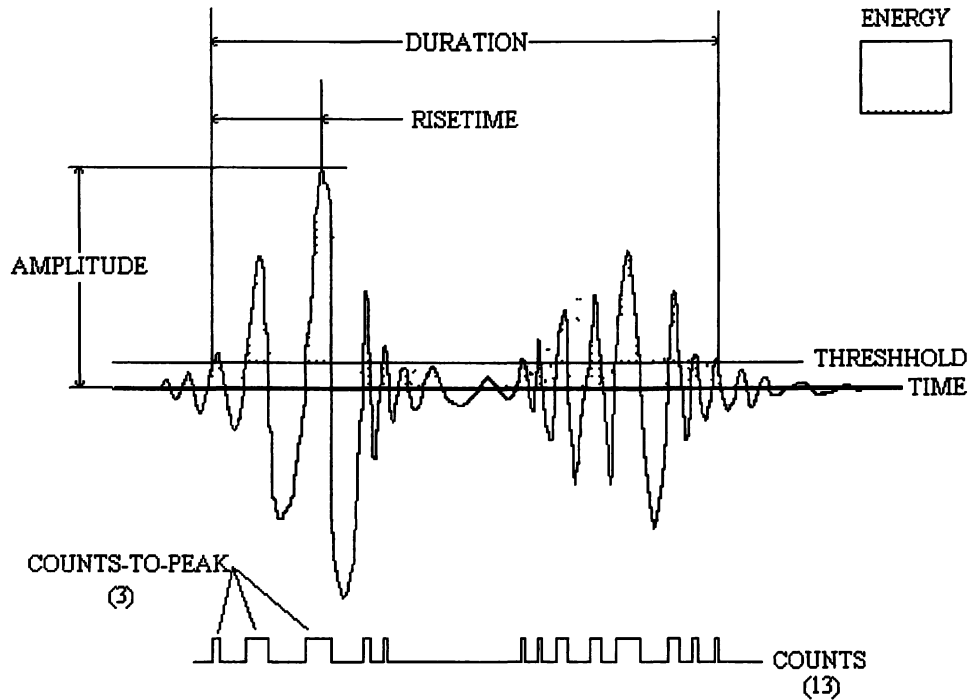
Figure 2.3 Acoustic Emission Parameters

Figure 2.3 depicts a voltage versus time signal from a piezoelectric sensor and the

associated AE quantification parameters. Amplitude is the maximum voltage (expressed in

decibels (dB)) of the incoming signal and is given by the equation, $A=20 \log(V/V_{ref})$, where

$V_{ref} = 1 \mu V$ at the sensor output. Counts is the number of times the voltage of the signal

crosses a threshold as set by the operator of the data acquisition system. By setting a high

threshold, background noise can be eliminated from analysis; by setting a low threshold, very

minute AE events can be detected, however, unless in a very quiet environment, these very

minute AE events can be lost in ambient noise. The duration is the time that the signal is

above the threshold. The energy is defined as the *Measured Area under the Rectified Signal*

Envelope (MARSE) and is shown as the shaded area in the figure. The risetime is the time it takes for the signal to reach its maximum amplitude. Finally the counts-to-peak parameter represents the number of counts that occur before the signal reaches its greatest amplitude.

2.1.2 HISTORICAL BACKGROUND

Acoustic emission nondestructive testing has been used to monitor in-flight fatigue crack growth in aircraft since 1979. The 7178-T6 aluminum lower wing skins of the C/KC-135 aircraft were experiencing severe fatigue cracking [Parrish]. This was due, in part, to the material properties of 7178-T6 aluminum, which is much more brittle than the 2024-T3 aluminum found on the Boeing 707 civilian counterpart of the C/KC-135. (The aircraft was designed so that it could still fly with a lower wing skin completely cracked as long as high load maneuvers were avoided.) Some aircraft, when inspected, were found to have cracks up to three inches long which were considered complete panel failures. To monitor this, an in-flight fatigue crack detection system was developed. The Acoustic Crack Detection System (ACDS) used in the C/KC-135 fleet was designed to warn the pilot with a light on the control panel when an incoming signal indicated unstable crack growth of 0.500 inch or longer.

In 1982, the upper wing trunnion of an Avro CF-100 was monitored using a single AE transducer [McBride and Maclachlan]. The wing trunnion is the major attachment point and load path between the wing and the fuselage. Analysis of the signals collected was performed on the ground after each flight. High amounts of fretting present blanketed the stable crack growth signals. Unstable crack growth signals were found to be 20 times greater in amplitude than stable crack signals for 4340 steel and at least 100 times greater for 7075-T6 aluminum. Therefore, the system allowed for the analysis of unstable crack growth only. Unstable crack growth is indicative of imminent failure. Crack growth becomes unstable when the rate of AE

activity goes from being roughly linear to being exponential

A second part of the Avro CF-100 research was to determine crack size with AE activity. Aircraft were flown which were known to have a crack in one wing trunnion and no crack in the other. By comparing the total amount of AE activity present in each trunnion during a flight, the ratio N_c/N_{uc} was created. This is the ratio of AE activity for the cracked trunnion to that of the uncracked trunnion. Using this quantity, they were able to provide reasonable estimates for crack size from just one hour of flight test data.

In 1987, a Mirage aircraft was monitored in flight using AE [Scala and Coyle]. Signal processing was used to filter out the fatigue cracks from the ambient noise. The lower wing spar was monitored using an array of sensors and a "fence" of guard sensors. The array of sensors allowed for determining the location of the AE source, and the guard sensors eliminated any events originating from locations outside of the area of interest. The semi-adaptive processing technique used to analyze the signals involved comparing "(i) features extracted by pattern recognition analysis of AE during aircraft monitoring and (ii) features predicted for the AE due to fatigue crack propagation."

For the C/KC-135 and the CF-100 aircraft discussed above, only unsteady crack growth could be detected due to the high level of ambient noise present during the testing. In the case of the Mirage aircraft, a semi-adaptive processing technique, including guard sensors, was employed after the test flights to both eliminate noise and to classify fatigue cracking. The next logical step would be to eliminate the use of guard sensors by the use of high speed, automatic computer processing of AE signals. This step could be accomplished by an AE data acquisition system which extracts the AE parameters from the sensor signals in

combination with a neural network capable of discerning the various types of failure mechanisms that produce the signals.

2.2 NEURAL NETWORKS

Neural networks are computer programs created to emulate the functioning of the human brain [Fausett]. Some uses of neural networks include classification, prediction, speech and voice recognition (classification), weather forecasting, data smoothing, and function approximation. Combinations of these uses are also possible. The type of neural network created depends upon its use.

For prediction, a back-propagation neural network is used. To train a back-propagation neural network, an input with a known output is supplied to the neural network. When the network outputs an answer, it is compared to the real answer. The error is then propagated back through the network to change the weights of the interconnecting links, hence the name *back-propagation* neural network. This is known as supervised learning.

For a classification problem with an unknown number of outcomes, unsupervised learning is used. In unsupervised learning, the output from the neural network must be matched with some known phenomenon, as in the case of this research where there are three distinct sources of acoustic activity: metal rubbing, rivet fretting, and fatigue crack propagation. The output must be matched to one of these classifications. This is done by knowing what physical phenomena are occurring during each phase of the test.

CHAPTER 3

SET-UP AND TESTING

3.1 EXPERIMENTAL SET-UP

3.1.1 PRESSURE VESSEL

The pressure vessel used for this research (Figure 3.1) was constructed from a sheet of 0.040 inch thick 2024-T3 aluminum rolled into a cylinder and secured between two steel endplates. The endplates were reinforced with steel braces to prevent deformation. Inside the cylinder was a sheet of PVC that acted as a bladder to prevent leaking. The vessel was held together with twelve 5/8 inch diameter threaded rods. One endplate had a threaded port to connect the hose for the hydraulic pump used to pressurize the vessel. The other endplate had a filling port, a port for a pressure transducer, and a port for a pressure gage.

The vessel was 12 inches long and 12 inches in diameter. To provide a stress concentration at which the fatigue crack was to initiate, a 1.0 inch diameter hole was cut into the cylinder. A notch (~3/16 inch long and 1/8 inch wide) was then filed on the side of the hole. An aluminum patch (Figure 3.2) was riveted under the hole to simulate a repair patch and to prevent the bladder from exiting the vessel. The rolled aluminum was held together by an overlapping joint with a double rivet line. The rivet lines were 0.625 inches apart with a rivet spacing of 0.400 inches. The PVC bladder was used to pressurize the vessel. The bladder was a cylinder approximately 16 inches long and 12 inches in diameter. The ends of

the bladder extended 2 inches beyond each end of the aluminum cylinder to form a seal

between the cylinder and the endplates.
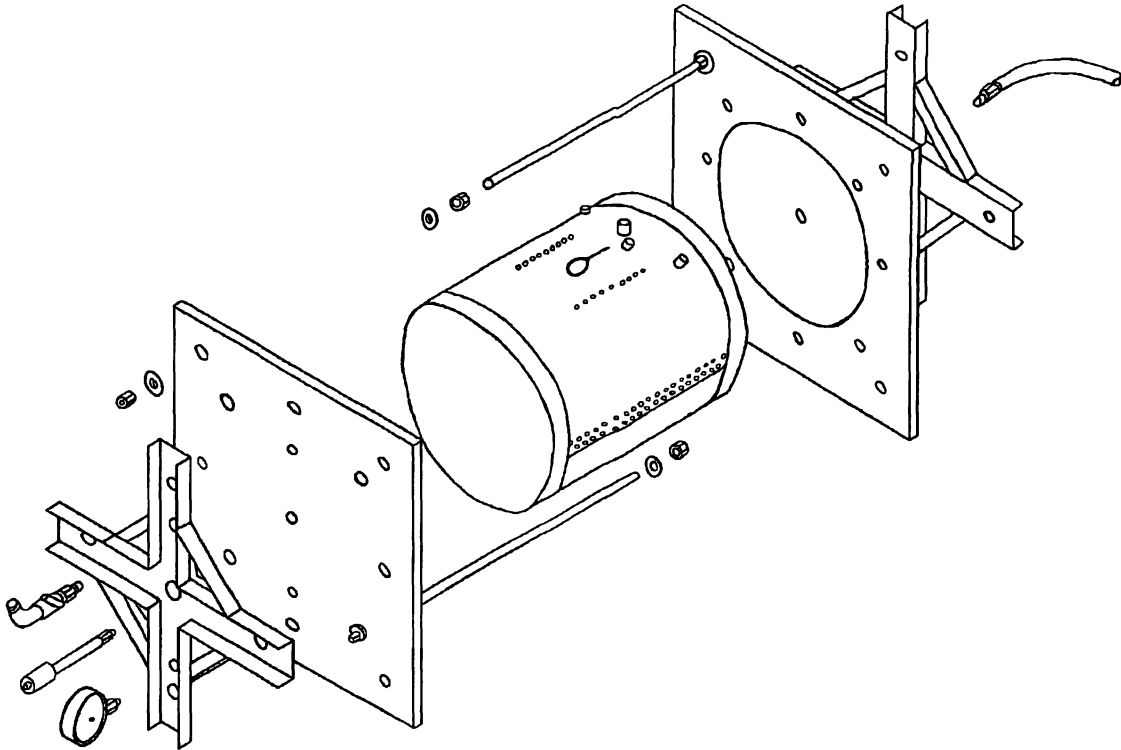
Figure 3.1 Exploded view of the pressure vessel
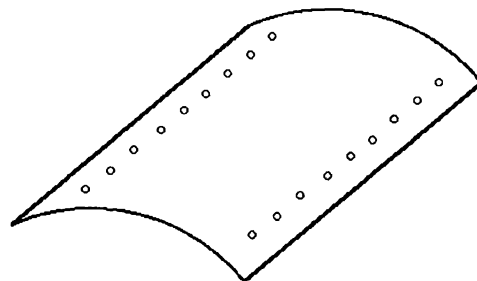
Figure 3.2 Enlarged view of the simulated repair patch

3.1.2 PRESSURIZATION

The vessel was filled with water using the filling port on the endplate. A hydraulic

pump (Figure 3.3) was placed in the grips of the Materials Testing System (MTS) machine

and then cycled to bleed air from the system. When the vessel was devoid of air, it was

sealed, then cyclically pressurized from 20 to 80 psi, first at 0.5 Hz and then at 1.0 Hz. The

sinusoidal pressurization cycle was generated by the MTS 410 Digital Function Generator

while the amplitude and zero were adjusted by hand to maintain the pressure span of 20 to 80

psi as read from the pressure gage (Figure 3.1). The function generator drove the actuator

on the MTS machine which forced the pump to a specific location, corresponding to a specific

change in pressure within the vessel.
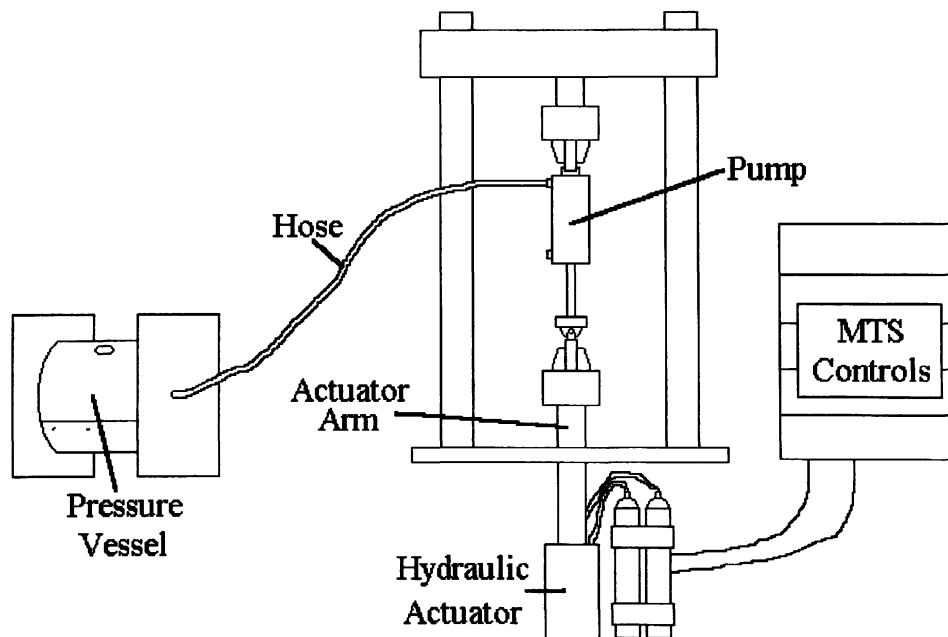
Figure 3.3 MTS and pressure vessel setup.

3.1.3 AE SENSORS

Three AE sensors were used to collect the waveforms emanating from the vessel. The sensors were 150 kHz resonant piezoelectric sensors. Through the course of the test, the sensors were repositioned from the patch to the rivet line and back to the patch to collect AE from metal rubbing, rivet fretting, and crack propagation, respectively (Figure 3.4). Three sensors were necessary to provide AE source location data for a previous research effort [Thornton], but only the data from the first hit sensor proved to be useful in this research. This is because as the stress waves propagate through the material, the characteristics of the wave change. If data from all three sensors were used, a single wave would register three times, once at each sensor, with a different set of parameters at each location. This would triple the number of events analyzed and possibly the number of failure types classified. The sensors were attached to the vessel with RTV, a silicone sealant, which acted as both an adhesive and an AE couplant, minimizing attenuation from the vessel to the sensor.

3.1.4 DATA ACQUISITION

The three AE sensors were attached through pre-amplifiers to the LOCAN-AT data acquisition system, which extracted the AE parameters from the signals (Figure 3.5). Again, the parameters extracted here were amplitude, counts, duration, energy, risetime, and count-to-peak. Once the test had begun, the LOCAN-AT collected data continuously from the vessel. The data were recorded and stored on three channels, one corresponding to each of the three sensors. The channel number, pressure, time, and date were also recorded along with the AE parameter data.

3.2 TESTING PROCEDURE

The starting and stopping of data collection was dictated by the need to clear the PC's

RAM drive and transfer waveform files from the RAM drive to a diskette. These stops in

a)

b)   c)
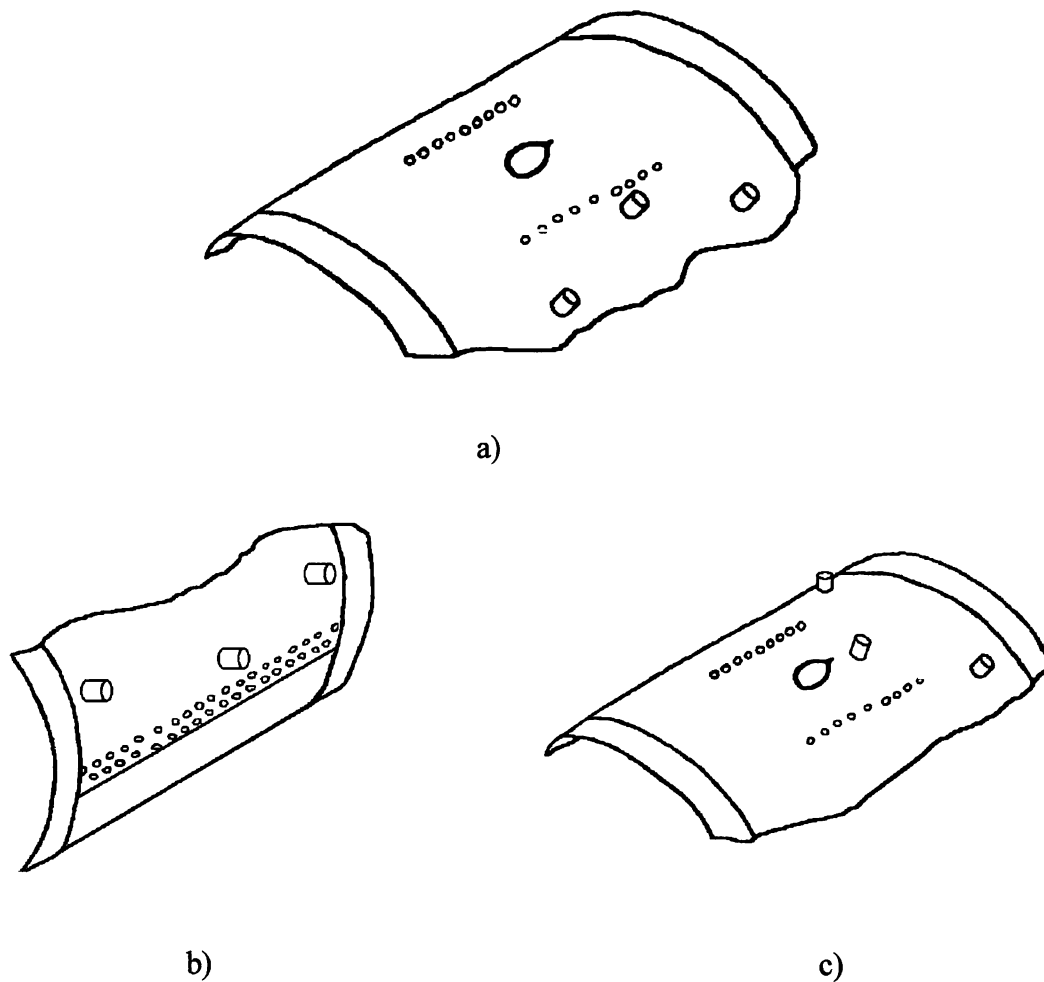
Figure 3.4 Placement of AE sensors for (a) metal plate rubbing, (b) rivet fretting, and (c) fatigue crack propagation

testing allowed the LOCAN-AT's data collection to be divided into small blocks which were

saved for subsequent processing and analysis. The testing, therefore, consisted of starting the

pressurization system, running the LOCAN-AT program, stopping the pressurization system,

transferring data files from the LOCAN-AT to a PC, checking the system for air, bleeding air from the system when necessary, and then restarting the test. After a sufficient amount of AE parameter data were collected for each mechanism, the test was stopped and the sensors moved to a new location. The test procedure was then repeated.
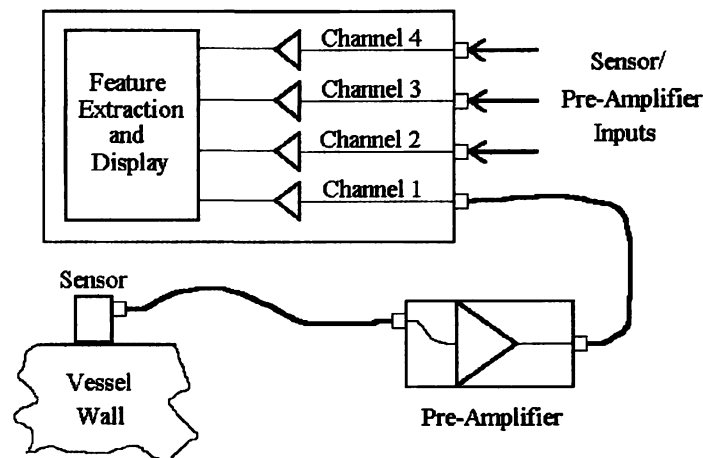
Figure 3.5 Schematic of the LOCAN-AT Data Acquisition System

To begin with, the sensors were placed over the patch to collect AE parameter data corresponding to the metal patch rubbing on the inside of the cylinder. Next, the sensors were moved to the rivet line to collect AE parameter data corresponding to rivet fretting. Lastly, the sensors were returned to the patch to collect AE parameter data corresponding to crack propagation. At each location on the vessel, the pressurization system was run at both 1.0 Hz and 0.5 Hz. This was done to provide a more comprehensive data set. Since the rate of crack growth is not constant in an aircraft, it was thought that using two different pressurization rates might better represent the fatigue cracking that actually occurs in an aircraft fuselage.

By having data for cracking at different pressurization rates, the test would more closely

resemble a real-life situation.

3.3 DATA PROCESSING

After the parameter data were collected by the LOCAN-AT, they were prepared for

use in the neural network. This was accomplished by first converting the LOCAN files from

their format to ASCII (which could be read by a spreadsheet program) using one of the

LOCAN's utilities called "atasc.exe." Next, the files were brought into a spreadsheet program

(Excel 5.0 for Windows) where all extraneous data (data in the files that are not AE

quantification parameters) were removed, leaving only the AE parameters and channel

number. Data from the wideband sensor and from the location sensors were deleted from the

data sets, so that only data from the first-hit sensor remained for analysis. Then a

representative data set was created using approximately one-third of the data files. These data

were used to train a SOM neural network to categorize the AE by similarities in their

parameter sets.

CHAPTER 4

NEURAL NETWORK ARCHITECTURE

4.1 ARCHITECTURE OF A SOM

A SOM generally consists of three layers: an input layer, a processing layer, which

contains processing elements (PEs), and an output layer (Figure 4.1). Each PE in the hidden

layer is connected to the output neurons and is fully interconnected to the other neurons in the

hidden layer. The 3 x 3 PE hidden layer shown here is considered to be a two-dimensional

layer. In general, the size of the hidden layer increases with the complexity of the data and the

number of inputs.
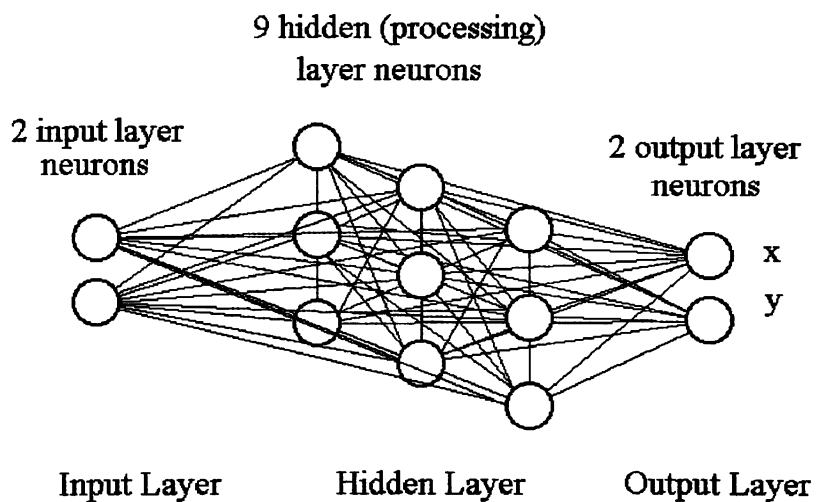
Figure 4.1 Example of a SOM architecture

The SOM classifies data with similar characteristics into groups. The actual numeric output for the SOM is in the form of an x and y coordinate. These coordinates are loaded into a supplemental program to plot the results. The typical output is a two-dimensional topographical map with clusters of points representing similar data.

4.2 AN EXAMPLE OF A SOM

One specific kind of classification neural network is the Kohonen self-organizing map (SOM), first developed by Teuvo Kohonen of the Helsinki University of Technology in the 1970s and early 1980s. These networks have been used in speech recognition and musical composition [Fausett] and incorporate unsupervised learning. In a Kohonen SOM, there are *m* PEs and the input signals are *n*-tulpes. In Kohonen learning, the input vector is compared to the weight vector, with the PE whose weight vector matches the input vector most closely being the "winner." This is also known as the shortest Euclidean distance. That PE and sometimes the PEs around it (called its neighbors) have their weights updated. The Kohonen algorithm is as follows [Walker and Hill]:

Step 1: Initialize weights (randomly between zero and one), set neighborhood, N,

learning rate, α, and momentum, γ

Step 2: Do while stopping condition is false

Step 3: For each input vector, x_1

Step 4: Compute for each PE

$$D_j = SQR((W_{ij} - x_i)^2) - \{ \gamma * (1/N - F_j) \}$$

Step 5: Find index "j" for D_j minimum

Step 6: Update all weights in neighborhood of "j"

$$W_{ij}(new) = W_{ij}(old) + \alpha(X_i - W_{ij}(old))$$

Step 7: Update learning rate and neighborhood parameters

Step 8: Test stopping condition

The variables of a SOM set by the user are the neighborhood size, the learning rate, and the momentum. The neighborhood (N) is the PEs around the "winning" PE whose weights are updated along with those of the "winner." A neighborhood of 1 means that only the weights of the "winner" are updated. If the N = 2, then the weights of the "winner" are updated, but so are the weights of the PEs adjacent to the "winner." The learning rate, α, dictates the increment the weights change during each pass through the algorithm. The momentum, γ, causes the non-winning PEs to be more competitive and therefore more likely to win in the next pass. The quantity F is the frequency that the PE in question has won.

For this example, there are three failure mechanism vectors that are used to train the 3 x 3 PE hidden layer SOM of Figure 4.1. Each input vector consists of an amplitude and a duration (both normalized between 0.00 and 1.00) and represents either unstable crack propagation, rivet fretting, or metal rubbing. The values below represent typical values for amplitude and duration for the three failure mechanisms, normalized to 100 dB maximum amplitude and 1 ms maximum duration.

Crack Propagation   (0.85, 0.15)
Rivet Fretting   (0.55, 0.35)
Metal Rubbing   (0.50, 0.90)

To begin with, let the neighborhood parameter, N, be 1.0, the learning coefficient, α,

be 0.20, and the momentum, γ, be zero. The example will go through several training passes

with all three vectors. Then let the original (randomized) weight vector be

$$
W_{ij} = \left|
\begin{array}{ccccccccc}
0.10 & 0.80 & 0.60 & 0.30 & 0.50 & 0.20 & 0.40 & 0.70 & 0.90 \\
0.50 & 0.40 & 0.30 & 0.80 & 0.90 & 0.50 & 0.60 & 0.20 & 0.70
\end{array}
\right|
$$

PE	i	ii	iii	iv	v	vi	vii	viii	ix

While the weights would normally be random numbers from 0.00 to 1.00, the initial weights in

this example are not random in order to simplify the calculations. Also for simplification, the

neighborhood parameter being set to zero means that only the weight of the winning PE will

be updated here and not that of the neighboring PEs. Input number 1 represents a crack

(0.85, 0.15). The Euclidean distances for this input are calculated as follows:

$$
\begin{array}{llll}
D(1) = & (W_{11} - x_1)^2 + & (W_{21} - x_2)^2 = & (0.1 - 0.85)^2 + & (0.5 - 0.15)^2 = & 0.685 \\
D(2) = & (W_{12} - x_1)^2 + & (W_{22} - x_2)^2 = & (0.8 - 0.85)^2 + & (0.4 - 0.15)^2 = & 0.065 \\
D(3) = & (W_{13} - x_1)^2 + & (W_{23} - x_2)^2 = & (0.6 - 0.85)^2 + & (0.3 - 0.15)^2 = & 0.085 \\
D(4) = & (W_{14} - x_1)^2 + & (W_{24} - x_2)^2 = & (0.3 - 0.85)^2 + & (0.8 - 0.15)^2 = & 0.725 \\
D(5) = & (W_{15} - x_1)^2 + & (W_{25} - x_2)^2 = & (0.5 - 0.85)^2 + & (0.9 - 0.15)^2 = & 0.685 \\
D(6) = & (W_{16} - x_1)^2 + & (W_{26} - x_2)^2 = & (0.2 - 0.85)^2 + & (0.5 - 0.15)^2 = & 0.545 \\
D(7) = & (W_{17} - x_1)^2 + & (W_{27} - x_2)^2 = & (0.4 - 0.85)^2 + & (0.6 - 0.15)^2 = & 0.405 \\
D(8) = & (W_{18} - x_1)^2 + & (W_{28} - x_2)^2 = & (0.7 - 0.85)^2 + & (0.2 - 0.15)^2 = & \mathbf{0.025} \\
D(9) = & (W_{19} - x_1)^2 + & (W_{29} - x_2)^2 = & (0.9 - 0.85)^2 + & (0.7 - 0.15)^2 = & 0.305
\end{array}
$$

PE #8 is the "winning" PE; therefore, PE #8's weights will be updated.

$$
\begin{array}{llllll}
W_{18}(new) = & W_{18}(old) + & \alpha\,(x_1 - W_{18}(old)) = & 0.7 + & 0.2(0.85 - 0.7) = & 0.73 \\
W_{28}(new) = & W_{28}(old) + & \alpha\,(x_2 - W_{28}(old)) = & 0.2 + & 0.2(0.15 - 0.2) = & 0.19
\end{array}
$$

The new weights for PE #8 are now 0.73 and 0.19, and the new weight vector then becomes

$$
W_{ij} = \left|
\begin{array}{ccccccccc}
0.1 & 0.8 & 0.6 & 0.3 & 0.5 & 0.2 & 0.4 & \mathbf{0.73} & 0.9 \\
0.5 & 0.4 & 0.3 & 0.8 & 0.9 & 0.5 & 0.6 & \mathbf{0.19} & 0.7
\end{array}
\right|
$$

PE	i	ii	iii	iv	v	vi	vii	viii	ix

Input number 2 represents a rivet (0.55, 0.35).

$D(1) = (W_{11} - x_1)^2 + (W_{21} - x_2)^2 = (0.1 - 0.55)^2 + (0.5 - 0.35)^2 = 0.225$

$D(2) = (W_{12} - x_1)^2 + (W_{22} - x_2)^2 = (0.8 - 0.55)^2 + (0.4 - 0.35)^2 = 0.065$

$D(3) = (W_{13} - x_1)^2 + (W_{23} - x_2)^2 = (0.6 - 0.55)^2 + (0.3 - 0.35)^2 = \mathbf{0.005}$

$D(4) = (W_{14} - x_1)^2 + (W_{24} - x_2)^2 = (0.3 - 0.55)^2 + (0.8 - 0.35)^2 = 0.265$

$D(5) = (W_{15} - x_1)^2 + (W_{25} - x_2)^2 = (0.5 - 0.55)^2 + (0.9 - 0.35)^2 = 0.305$

$D(6) = (W_{16} - x_1)^2 + (W_{26} - x_2)^2 = (0.2 - 0.55)^2 + (0.5 - 0.35)^2 = 0.145$

$D(7) = (W_{17} - x_1)^2 + (W_{27} - x_2)^2 = (0.4 - 0.55)^2 + (0.6 - 0.35)^2 = 0.085$

$D(8) = (W_{18} - x_1)^2 + (W_{28} - x_2)^2 = (0.73 - 0.55)^2 + (0.19 - 0.35)^2 = 0.058$

$D(9) = (W_{19} - x_1)^2 + (W_{29} - x_2)^2 = (0.9 - 0.55)^2 + (0.7 - 0.35)^2 = 0.245$

Here PE #3 is the "winning" PE, so its weights will be updated.

$W_{13}(\text{new}) = W_{13}(\text{old}) + \alpha (x_1 - W_{13}(\text{old})) = 0.6 + 0.2(0.55 - 0.6) = 0.59$

$W_{23}(\text{new}) = W_{23}(\text{old}) + \alpha (x_2 - W_{23}(\text{old})) = 0.3 + 0.2(0.35 - 0.3) = 0.31$

The new weight vector becomes

$W_{ij} =$	0.1	0.8	**0.59**	0.3	0.5	0.2	0.4	0.73	0.9
	0.5	0.4	**0.31**	0.8	0.9	0.5	0.6	0.19	0.7
PE	i	ii	iii	iv	v	vi	vii	viii	ix

The third input, which represents metal rubbing, is (0.45, 0.35).

$D(1) = (W_{11} - x_1)^2 + (W_{21} - x_2)^2 = (0.1 - 0.50)^2 + (0.5 - 0.90)^2 = 0.3200$

$D(2) = (W_{12} - x_1)^2 + (W_{22} - x_2)^2 = (0.8 - 0.50)^2 + (0.4 - 0.90)^2 = 0.3400$

$D(3) = (W_{13} - x_1)^2 + (W_{23} - x_2)^2 = (0.59 - 0.50)^2 + (0.31 - 0.90)^2 = 0.3562$

$D(4) = (W_{14} - x_1)^2 + (W_{24} - x_2)^2 = (0.3 - 0.50)^2 + (0.8 - 0.90)^2 = 0.0500$

$D(5) = (W_{15} - x_1)^2 + (W_{25} - x_2)^2 = (0.5 - 0.50)^2 + (0.9 - 0.90)^2 = \mathbf{0.0000}$

$D(6) = (W_{16} - x_1)^2 + (W_{26} - x_2)^2 = (0.2 - 0.50)^2 + (0.5 - 0.90)^2 = 0.2500$

$D(7) = (W_{17} - x_1)^2 + (W_{27} - x_2)^2 = (0.4 - 0.50)^2 + (0.6 - 0.90)^2 = 0.1000$

$D(8) = (W_{18} - x_1)^2 + (W_{28} - x_2)^2 = (0.73 - 0.50)^2 + (0.19 - 0.90)^2 = 0.5570$

$D(9) = (W_{19} - x_1)^2 + (W_{29} - x_2)^2 = (0.9 - 0.50)^2 + (0.7 - 0.90)^2 = 0.2000$

Here the winning PE is PE #5, so its weights are updated. In this case the weights match the input exactly, so the weights do not actually change. In summary, the weight vector after the first pass of the three input data vectors becomes

$W_{ij} =$	0.1	0.8	**0.59**	0.3	**0.5**	0.2	0.4	**0.73**	0.9
	0.5	0.4	**0.31**	0.8	**0.9**	0.5	0.6	**0.19**	0.7
PE	i	ii	iii	iv	v	vi	vii	viii	ix

Hence, after one training pass, it appears as though PE #3 represents rivet fretting, PE

5 represents metal rubbing, and PE #8 represents fatigue crack growth. Continuing, after

five passes, the weight vector becomes

$$W_{ij} = \begin{vmatrix} 0.1 & 0.8 & 0.566384 & 0.3 & 0.5 & 0.2 & 0.4 & 0.800848 & 0.9 \\ 0.5 & 0.4 & 0.333616 & 0.8 & 0.9 & 0.5 & 0.6 & 0.166384 & 0.7 \end{vmatrix}$$

| PE | i | ii | iii | iv | v | vi | vii | viii | ix |

After 10 passes,

$$W_{ij} = \begin{vmatrix} 0.1 & 0.8 & 0.5553687 & 0.3 & 0.5 & 0.2 & 0.4 & 0.8338939 & 0.9 \\ 0.5 & 0.4 & 0.3446313 & 0.8 & 0.9 & 0.5 & 0.6 & 0.1553687 & 0.7 \end{vmatrix}$$

| PE | i | ii | iii | iv | v | vi | vii | viii | ix |

After 20 passes,

$$W_{ij} = \begin{vmatrix} 0.1 & 0.8 & 0.5505765 & 0.3 & 0.5 & 0.2 & 0.4 & 0.8482707 & 0.9 \\ 0.5 & 0.4 & 0.3494236 & 0.8 & 0.9 & 0.5 & 0.6 & 0.1505756 & 0.7 \end{vmatrix}$$

| PE | i | ii | iii | iv | v | vi | vii | viii | ix |

After 50 passes,

$$W_{ij} = \begin{vmatrix} 0.1 & 0.8 & 0.5500007 & 0.3 & 0.5 & 0.2 & 0.4 & 0.8499979 & 0.9 \\ 0.5 & 0.4 & 0.3499993 & 0.8 & 0.9 & 0.5 & 0.6 & 0.1500007 & 0.7 \end{vmatrix}$$

| PE | i | ii | iii | iv | v | vi | vii | viii | ix |

And after 100 passes,

$$W_{ij} = \begin{vmatrix} 0.1 & 0.8 & 0.5500001 & 0.3 & 0.5 & 0.2 & 0.4 & 0.8499999 & 0.9 \\ 0.5 & 0.4 & 0.3499999 & 0.8 & 0.9 & 0.5 & 0.6 & 0.15 & 0.7 \end{vmatrix}$$

| PE | i | ii | iii | iv | v | vi | vii | viii | ix |

Note that between 50 and 100 passes the weight vector did not change significantly. After

1,000 passes, the weight vector was identical to that after 100 passes: there was no further

change.

Now that this sample SOM is trained, if a large data set made up of vectors like the

input vectors were input to the SOM (not training, but testing), the output would look

something like Figure 4.2, which shows the 2-D output of this SOM. If the output were

transformed into three dimensions, the output would look like Figure 4.3, which shows that

there were approximately equal amounts of metal rubbing and rivet fretting signals, and a

smaller number of fatigue crack growth signals.
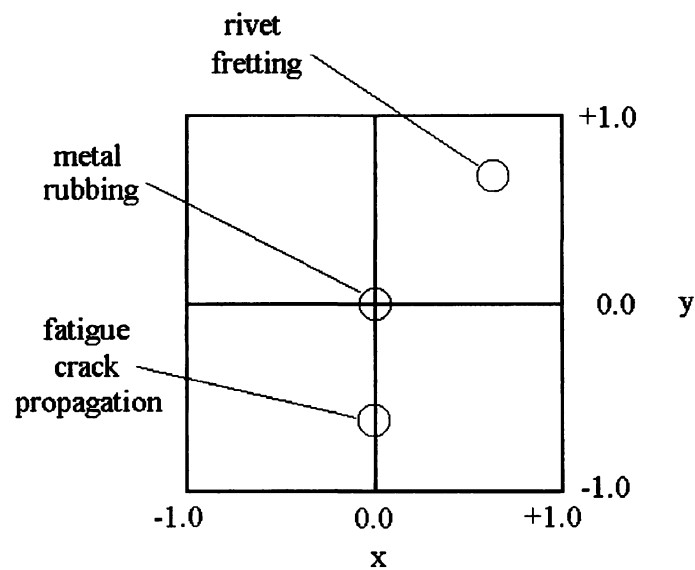
Figure 4.2 2-D output from the example SOM
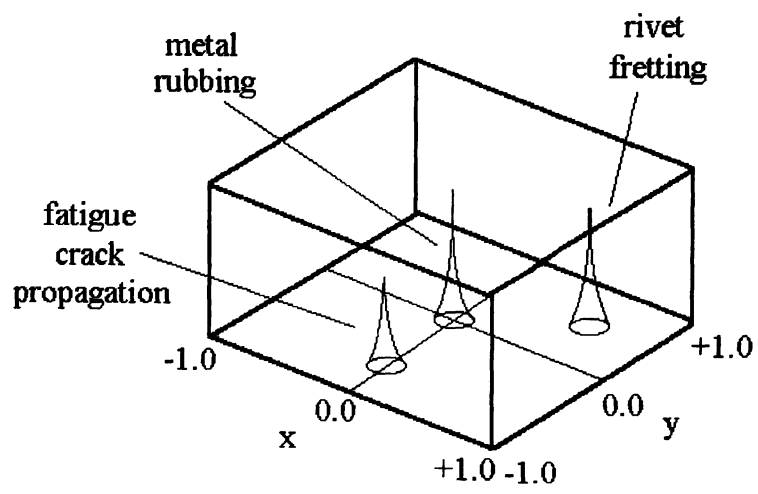
Figure 4.3 3-D output from the example SOM.

CHAPTER 5

ANALYSIS AND VERIFICATION OF RESULTS

A neural network software package called *Neural Networks Professional II / Plus* was used to create the neural networks used in this research. A series of self-organizing maps (SOMs), each having a slightly different architecture, were used to classify the modes of failure occurring in the research vessel. The first set of SOMs used data from all three AE sensors. These networks employed all six AE parameters as inputs with a 30 x 30 processing element (PE) hidden layer, then five of the six AE parameters (counts-to-peak was eliminated) with a 30 x 30 PE hidden layer. The second set of SOMs used input data from only one sensor (the sensor closest to the AE source) and all six AE parameters; hidden layer sizes employed were 20 x 20, 25 x 25, and 30 x 30 PEs. By increasing the size of the hidden layer, the resolution of the SOM increases. The third and final set of networks used one sensor and a 2 x 2 PE hidden layer (4 PEs), which forced the output to be one of four possible outcomes. Five such networks were created, but only three of them provided meaningful results. Of these, the first SOM in this set used three input parameters: risetime, duration, and amplitude. The second SOM used all six AE parameters, and the last SOM used energy, duration and amplitude as input parameters.

5.1 INITIAL RESULTS

The first set of SOMs used inputs from all three sensors on the vessel. The results

from these SOMs were a smear of (x, y) coordinates on the Cartesian plane (Figure 5.1). No

distinct clustering of data could be discerned. The (x, y) coordinates were run through a

computer program called "z-coord2.bas" which transformed the (x, y) coordinates into (x, y,

z) coordinates, with the z-coordinate being the frequency of occurrence of each (x, y) point.

This new output then provided surface plots. These plots contained several peaks

Figure 5.1 Inconclusive initial SOM output.

corresponding to clusterings of input parameters; however, there were too many peaks

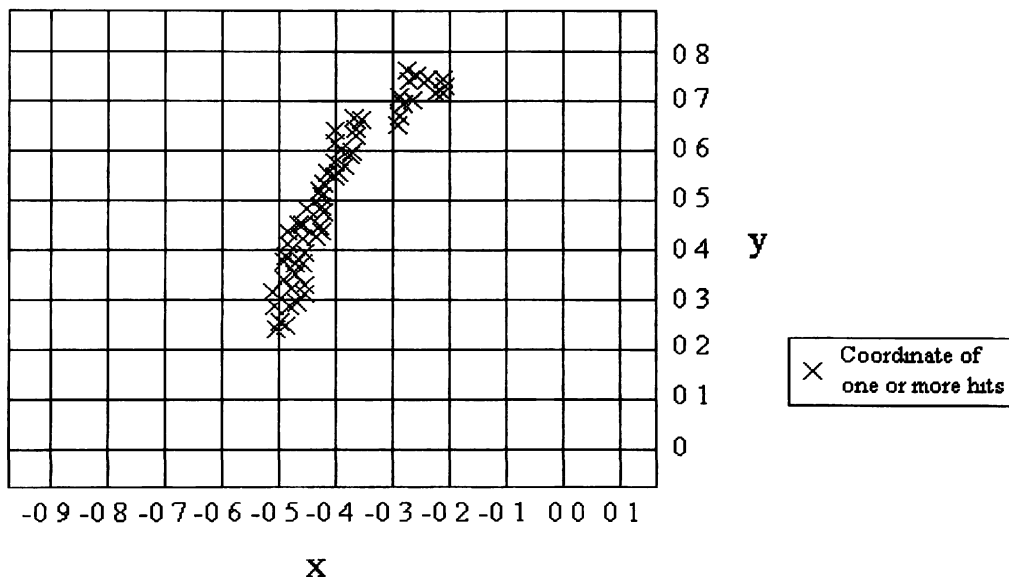present to define any of the peaks as rubbing, rivet fretting, or fatigue crack growth. This

occurred because as a stress wave propagates through the vessel its parameters change due to

dispersion. Each sensor therefore recorded a different set of parameters for the same AE

wave. Consequently, the SOM classified the data it received into more than nine clusters with at least three clusters per sensor.

5.2 INTERMEDIATE RESULTS

Since the use of inputs from all three sensors provided too much scatter in the data, a second set of SOMs was created that used input from only one sensor. This avoided the problem of having the same wave classified at three different output locations. The first of these SOMs used all six AE parameters and a 20 x 20 PE hidden layer (400 PEs). The output was a surface plot with three major peaks and several smaller peaks. It is believed that the larger peaks corresponded to rubbing, rivet fretting, and crack propagation, but there were so many other peaks present that it was hard to determine what was what.

A second SOM was created using only five of the AE parameters (counts-to-peak was dropped). The output of this SOM was like that of the first, only worse. The next step was to use all six parameters, but now in a SOM with a 25 x 25 PE hidden layer (625 PEs). The increase in hidden layer PEs resulted in greater resolution. The surface plot from this SOM was much flatter, with only a few sharp, distinct peaks. Correlating the peaks to failure mechanisms was again difficult due to the presence of more than three peaks.

A third SOM was formed with a 30 x 30 PE hidden layer (900 PEs). This was the best SOM in the second series. The resulting surface plot shown in Figure 5.2 is relatively flat with a series of very distinct peaks. From this plot, one can deduce that the first peak from the left corresponds to metal rubbing, the second peak corresponds to fatigue crack growth, and the third (and fourth) peaks correspond to rivet fretting from the two rivet lines in the lap joint. There are, however, still some smaller peaks that cannot be labeled.

M4B–RUB

M4B–RIV

M4B–CRK
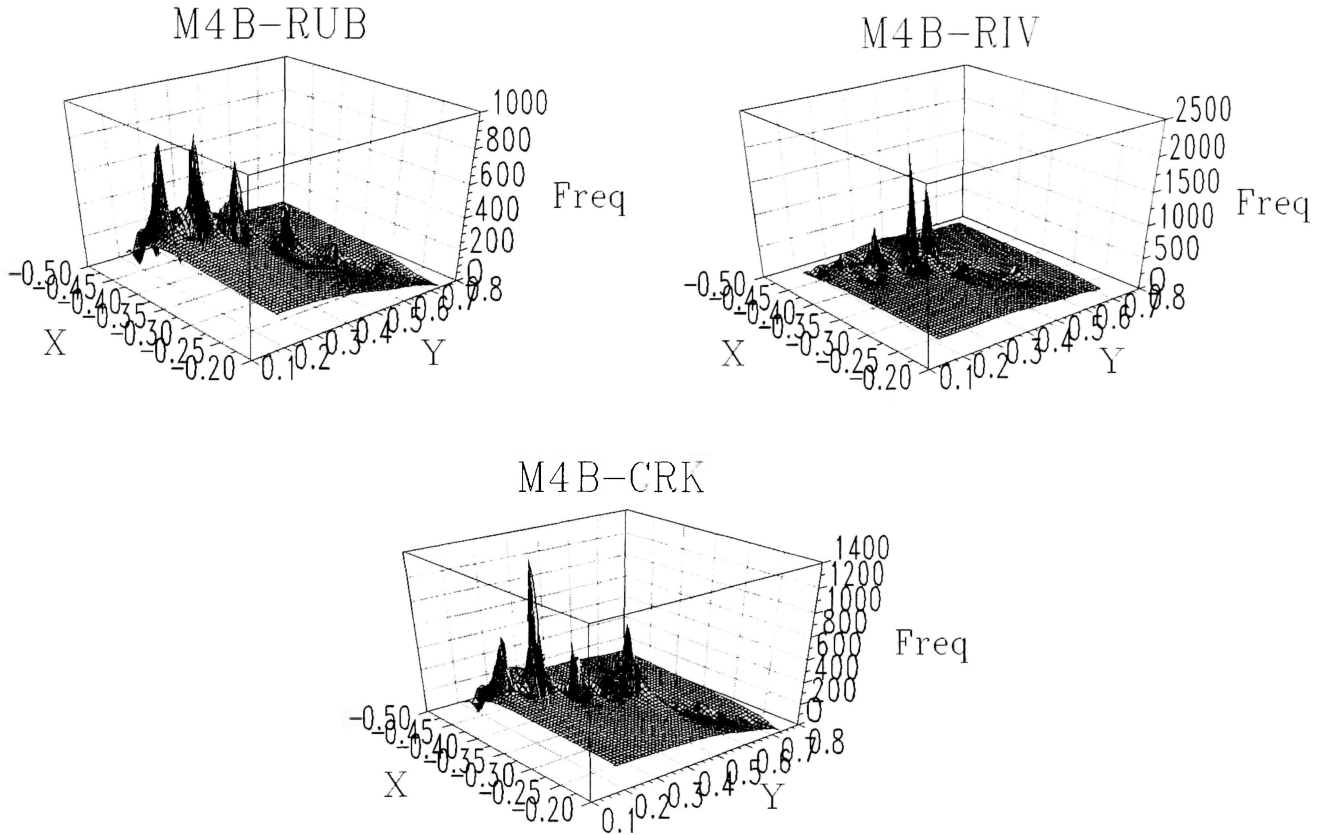
Figure 5.2 Final 3-D output from 30 x 30 PE hidden layer SOM.

5.3 FINAL RESULTS

After training and testing a series of neural networks with very large hidden layers, it

was decided to try a SOM with only four hidden layer PEs. This would give the SOM only

four choices in which to place a set of parameters (since there were only three AE source

mechanisms present). This would prevent duplicate classification. The SOMs with the smaller

hidden layers forced each data set into one of four classifications. This eliminated the

phenomenon of having more than one set of output coordinates for the same source

mechanism, such as rivet fretting from the two rivet lines on the vessel showing up at two different coordinates.

The final series of five SOMs all had a 2 x 2 PE hidden layer (4 PEs), while the size of the input layer changed. Two SOMs used only selected AE parameters. The initial SOM (M5) used risetime, duration, and amplitude as the input parameters. Another SOM in the series (M7) used all six AE parameters. The final SOM (M9) used energy, duration, and amplitude as the input parameters. Historically, some AE parameters are better for the classification of failure mechanisms than others. For example, energy is a good classification parameter because the energy of a wave packet does not change as the wave propagates through a plate or shell-type structure, though the amplitude will diminish and the duration will increase due to dispersion [Pollock]. Previous research ([Kouvarakos and Hill] and [Ely and Hill]) showed that duration is a very useful parameter when classifying failure mechanisms in tensile test specimens. Amplitude is often used as a classifier as well when the structure is relatively small and the effect of dispersion is negligible [Hill, Walker, and Rowell]. Stable fatigue crack growth has a very low amplitude with respect to other failure mechanisms, such as rivet fretting [McBride and Maclachlan], and therefore was included as a defining parameter here.

The initial output of the last of these SOMs looked like the plot in Figure 5.3 below. Once the x-y plot was produced, it was observed that each of the three outputs had its own distinct x-coordinate. Therefore one could produce a histogram of the x-coordinate frequencies to determine how often a set of AE parameters was classified at each coordinate. This was done to determine which set of (x, y) coordinates corresponded to which failure

mechanism. This also required less data reduction than producing a three-dimensional surface

plot.
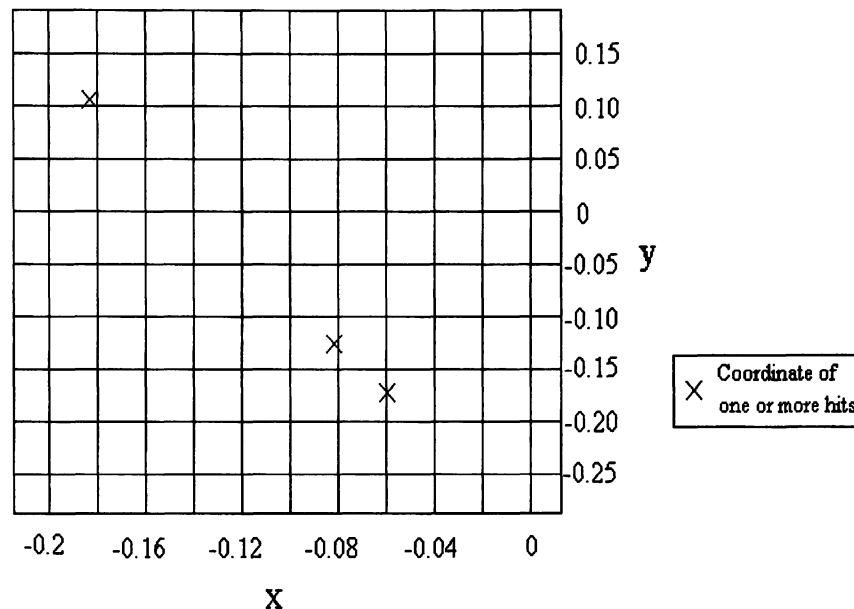
Figure 5.3 Initial output from a SOM with a 2 x 2 PE hidden layer.

The x-coordinate histograms for each of the three AE parameters from SOM M5 are

pictured in Figure 5.4 below. As the sensor was moved from one location to another on the

pressure vessel, the main source of AE changed. This becomes most evident for the plot

labeled "M5-CRK.DAT" in Figure 5.4. The parameter data that resulted in this plot were

collected from the repair patch after a fatigue crack was visually verified. Previous research

[Thornton] showed that a fatigue crack had initiated at the onset of the test and was located at

the rivet line. The SOM classified these signals along with the rubbing and rivet fretting

signals. By the end of the test, the fatigue crack had become the most active AE source.

While data were being collected for metal rubbing, a fatigue crack had already

initiated, which was not visually detected. The SOM, however, picked out both the crack and

the rubbing data. Also, while AE were being collected for crack propagation, the metal plate
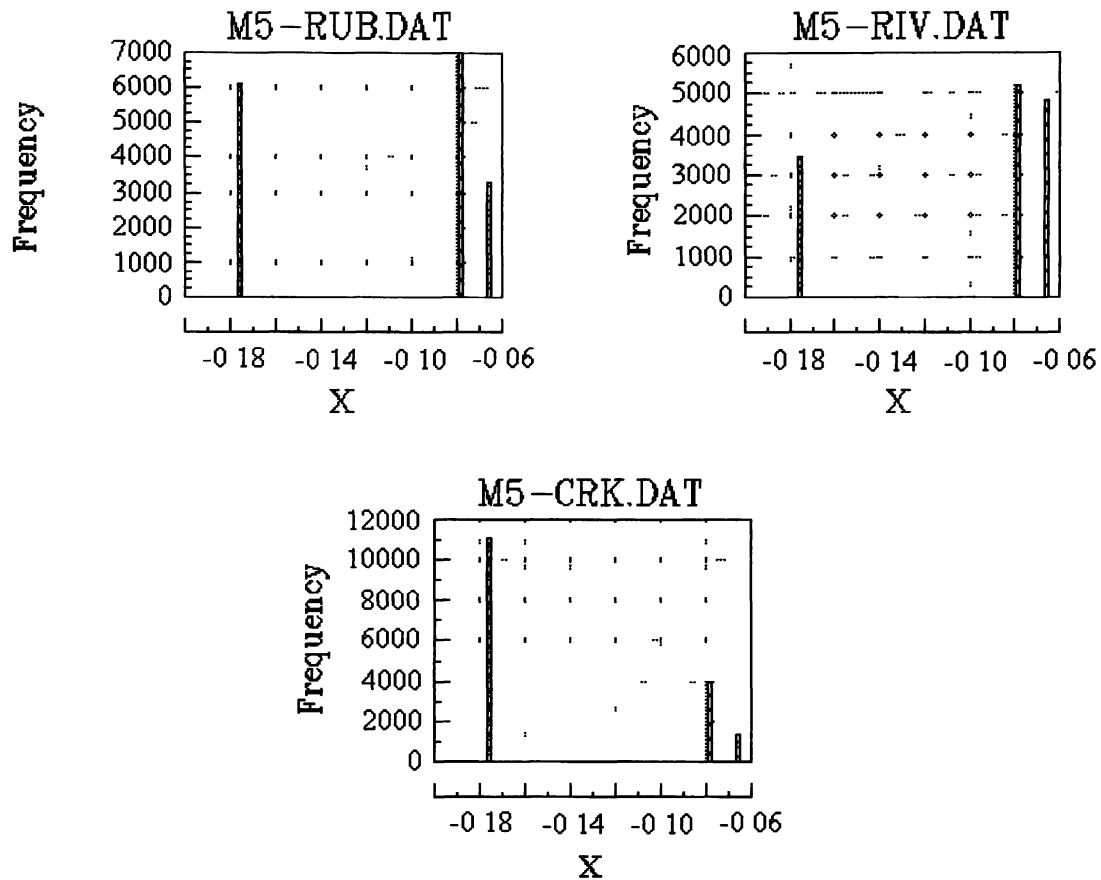
Figure 5.4 Final output from SOM M5.

was still rubbing. These different AE sources appeared as separate coordinates in the final

output. Matching these coordinates to their failure modes was accomplished by comparing

their histogram values at different times during the testing. In the early phases of the test, the

main source of AE was the metal rubbing ("rub"). When the sensors were placed near the

rivet line ("riv"), it was originally thought that only signals for rivet fretting would be collected; however, metal rubbing and crack growth were not only found to be present but were more prevalent than rivet fretting. Moreover, a fatigue crack was visually verified in one of the rivet holes after testing was completed. When the sensors were moved back to the repair patch after the data for rivet fretting were recorded, the main source of AE was the propagation of the fatigue crack ("crk"), which was the largest of the histograms in the output for that phase of the test. Thus the (x, y) coordinates from SOM M5 for each of the three source mechanisms (Figure 5.4) were found to be: rubbing, x = - 0.082, y = - 0.173; rivet fretting, x = - 0.060, y = - 0.124; and stable crack propagation, x = - 0.182, y = 0.104.

The outputs from each of the 2x2 hidden layer SOMs were compared and used to determine which sets of AE parameters correlated with the three (x, y) coordinates from Figure 5.3. The classification provided by these three networks were virtually identical, with only a few misclassifications (Table 5.2). These were probably caused by multiple hits. For example, if fatigue cracking and rivet fretting occurred simultaneously, or at least within a few microseconds of each other, the data acquisition system would record the two hits as one with the overall AE parameters being combinations of the two sources.

Once the three failure mechanisms (output coordinates) were matched to their respective input parameters, AE parameter distributions were generated for each failure mechanism. These are presented below in Figures 5.5 to 5.10. Each figure contains histograms for a given AE parameter for each failure mechanism (rubbing, rivet fretting, crack propagation).

From the histograms it can be seen that the risetimes for fatigue crack growth are usually less than 20 μs but may be as high as 50 μs. Risetimes for rivet fretting typically range

from 1 to 110 μs, while risetimes for metal rubbing range from 1 to 150 μs. Thus, if the

risetime for a signal were say, 80 μs, it would be safe to conclude that the signal in question

would not be a fatigue crack.
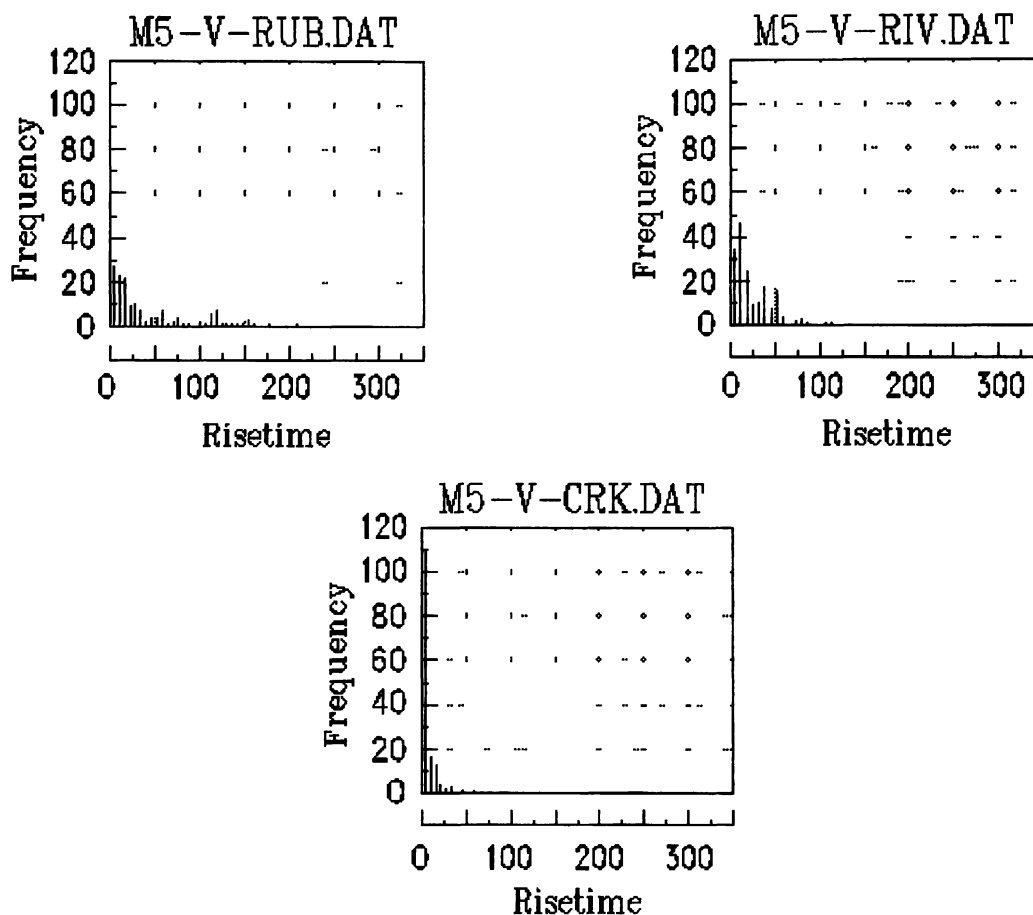
Figure 5.5 Risetime distributions for the three AE source mechanisms.

As can be seen in Figure 5.6, the AE counts for a crack signal are typically between 1

and 5. Counts for rivet fretting extend from 1 to 40, while counts for metal rubbing range

from 1 to 100. One would expect that the AE counts for cracking signals would be low, since

the propagation of a fatigue crack occurs in short, distinct steps, unlike rivet fretting or metal

rubbing, which are long, drawn-out events in comparison. This same kind of thinking can be

extended to the other AE parameters, such as risetime, energy, and duration, where the same

relationships hold.
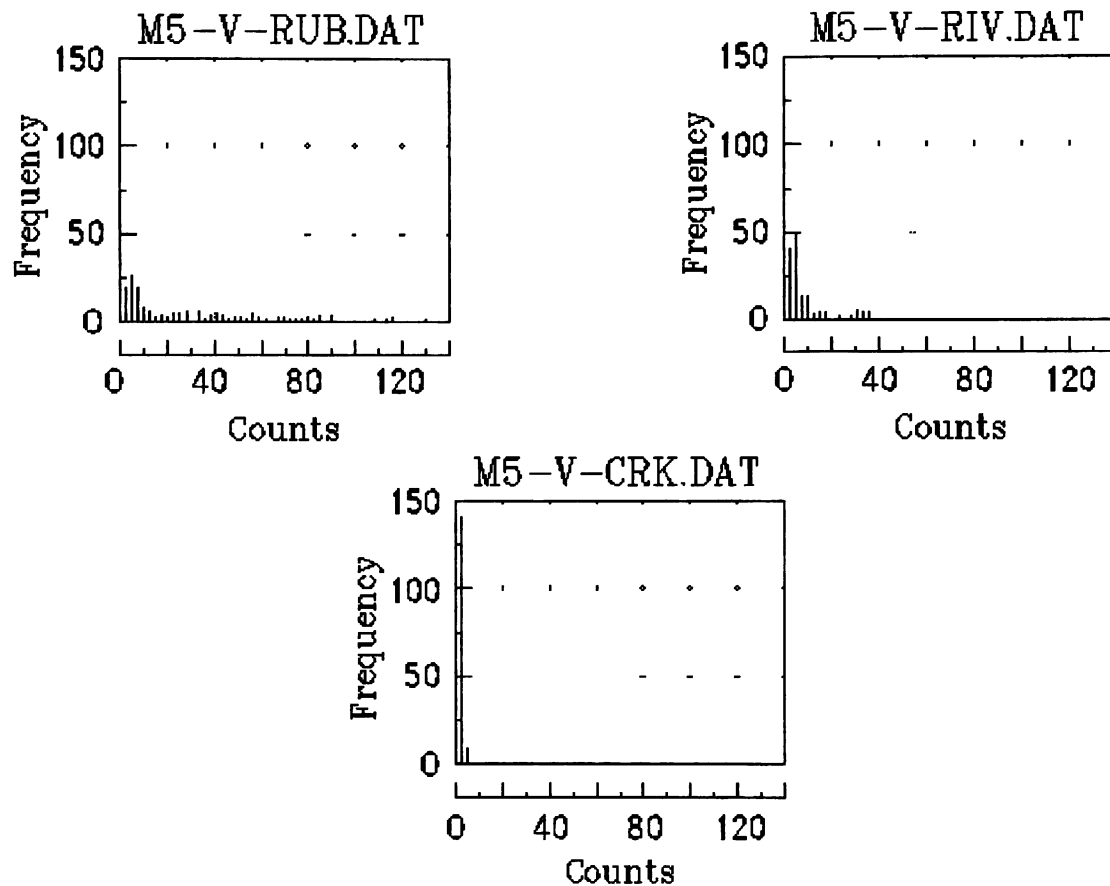
Figure 5.6 Counts distributions for the three AE source mechanisms.

In Figure 5.7 the energy distributions for the three failure mechanism are shown.

Notice that the energy for a fatigue crack is zero. This is due to the short, distinct nature of

fatigue crack propagation. Rivet fretting is a slightly longer process and therefore has more

energy. Rubbing is characteristically a long duration event and therefore has a lot of energy.
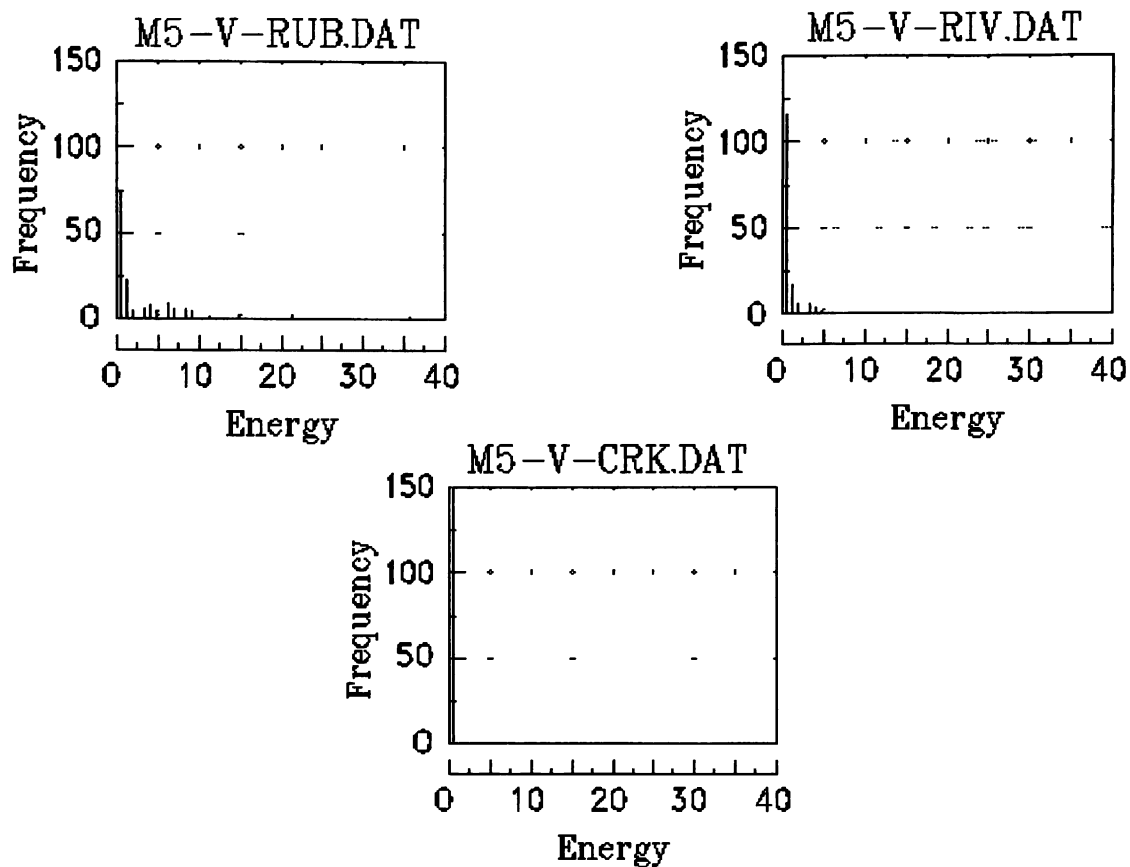
Figure 5.7 Energy distributions for the three source mechanisms.

Figure 5.8 below depicts the duration distributions for the three source mechanisms.

As stated previously, the durations for crack propagation are very short; here it can be seen

that crack durations are less than 55 μs. Signals for rivet fretting have durations between 30

and 625 μs, and metal rubbing signals may last anywhere from 144 to 2081 μs. Signals with

durations over 1000 μs are most likely multiple hits being recorded as a single hit.

M5-V-RUB.DAT

M5-V-RIV.DAT

M5-V-CRK.DAT
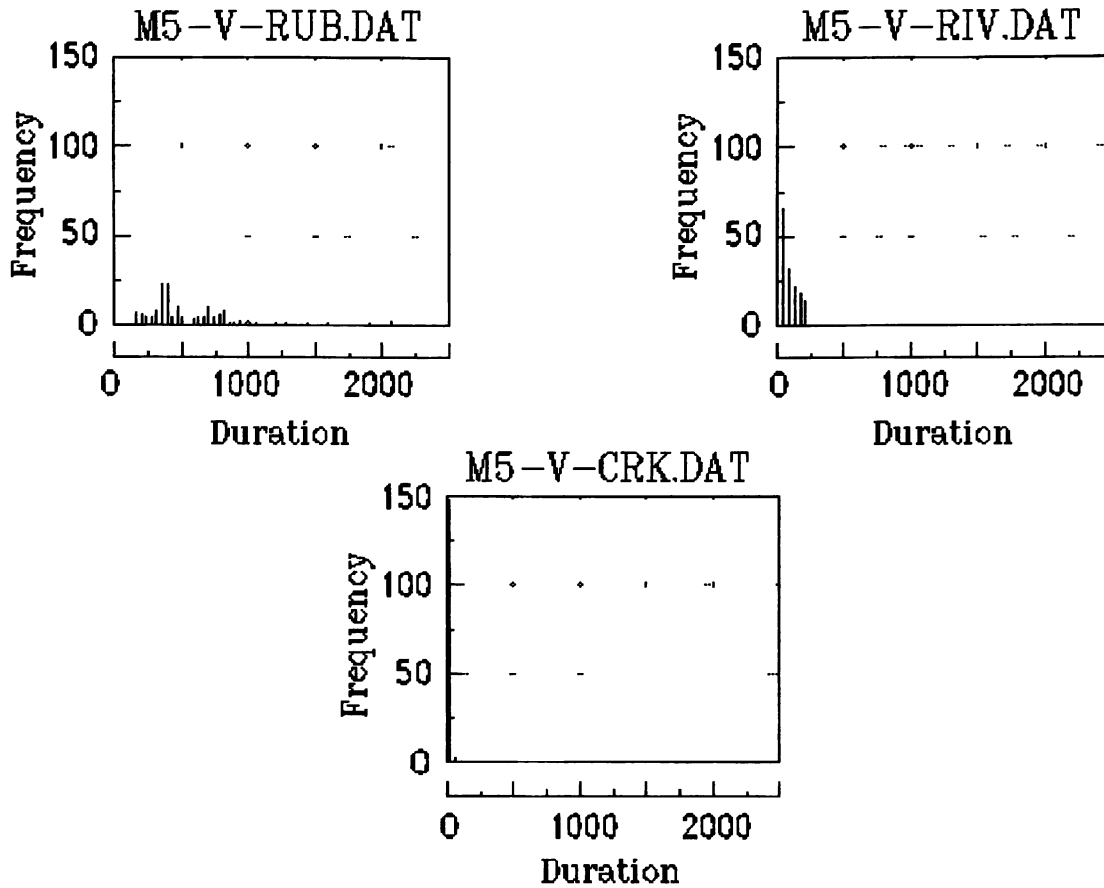
Figure 5.8 Duration distributions for the three source mechanisms.

The amplitude distributions for the three source mechanisms are plotted in Figure 5.9. As anticipated, the amplitudes for the stable fatigue crack growth were noticeably lower than those of the other AE sources in the vessel. While amplitude was originally thought to be a good parameter for the separation of failure mechanisms, one can see that there is a lot of overlap between the three different sources. For example, every source has at least one hit with an amplitude of 40 dB. The crack signals remained below 50 dB except for a few, while signals for metal rubbing and rivet fretting have amplitudes above 60 dB.
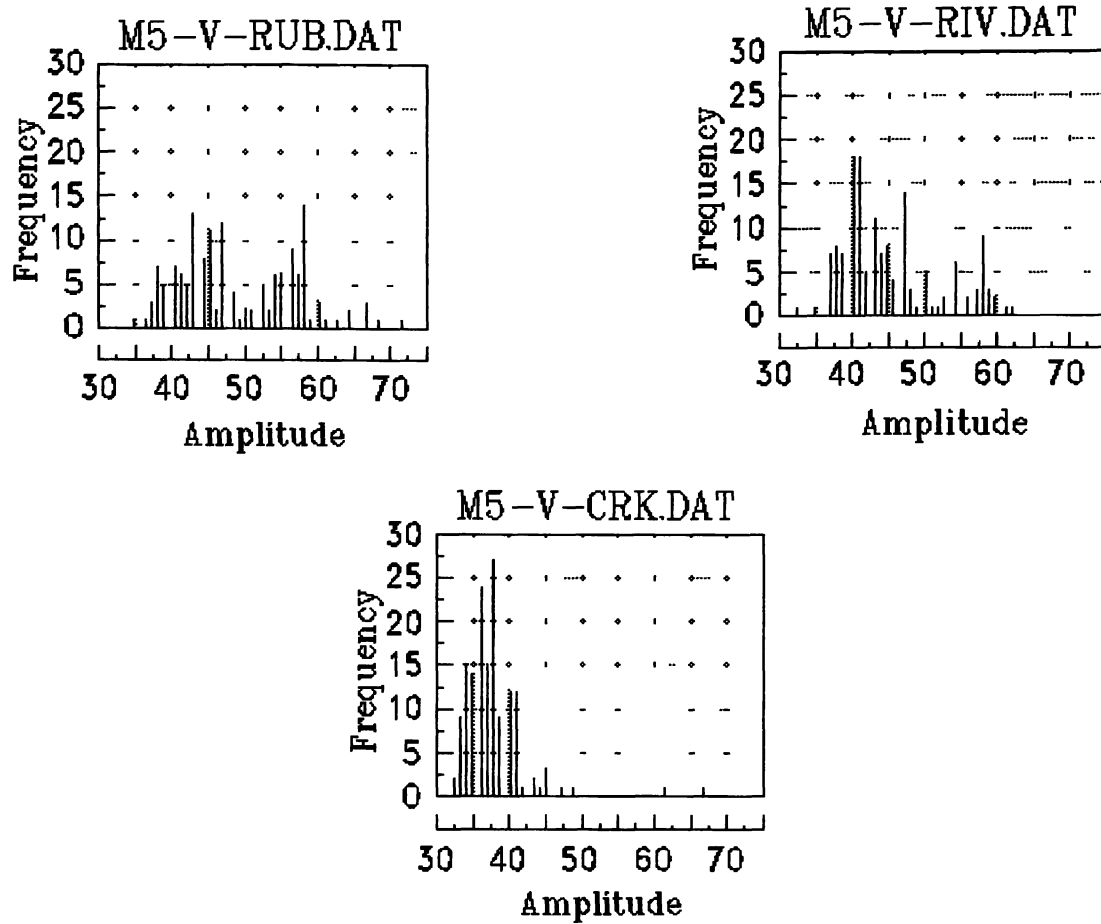
Figure 5.9 Amplitude distributions for the three source mechanisms.

As can be seen in Figure 5.10, the counts-to-peak parameter for fatigue crack growth

remains under 6. This follows directly from the counts parameter. The counts-to-peak

parameter may be as high as 34 for the other two source mechanisms (whose total counts may

exceed 100). This means that if the counts-to-peak value is greater than 6, the event in

question is probably not a fatigue crack.
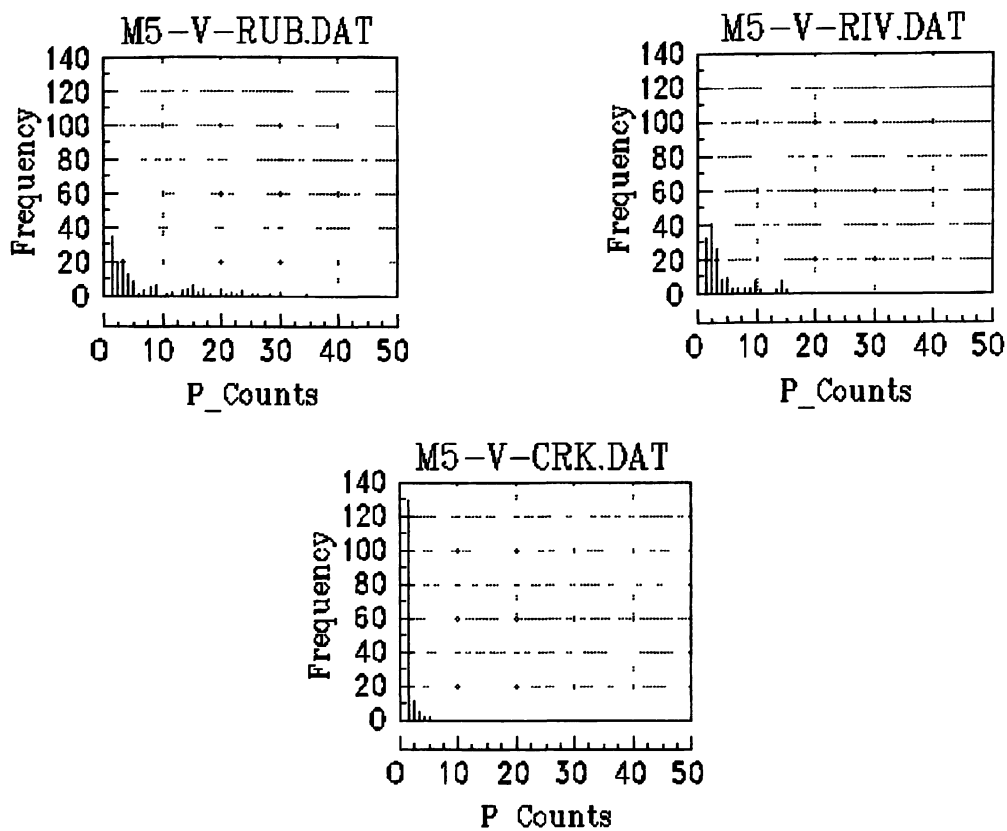
Figure 5.10 Counts-to-Peak distributions for the three source mechanisms.

Finally, the AE parameters fall within certain ranges, depending upon the failure

mechanism that causes them. These ranges are defined in Table 5.1. From this it can be seen

that the AE parameter having the greatest separation for the three failure mechanisms is

duration. Risetime, counts, energy, and counts-to-peak all provide approximately the same

information. Because of the overlap in ranges, amplitude would appear to provide the least

discrimination of all the AE parameters.

Table 5.1 Ranges for AE parameters from each source mechanism.

Parameter	Fatigue Cracking	Rivet Fretting	Rubbing
Risetime (μs)	1 - 65	1 - 301	1 - 207
Counts	1 - 8	1 - 78	1 - 130
Energy	0	0 - 9	0 - 36
Duration (μs)	1 - 55	30 - 628	144 - 2081
Amplitude (dB)	32 - 67	32 - 62	35 71
Counts-to-Peak	1 - 6	1 - 47	1 - 35

Table 5.2 contains a small sample of AE parameters used as input to test the last series

of neural networks. The SOM with the least amount of misclassified signals was M5. SOM

M7 had several misclassified signals, but most of these were between rivet fretting and

rubbing signals. SOM M9 had a few misclassified signals. Note that the misclassifications are

indicated in bold type.

A final test group was generated using 600 AE hits. The SOM outputs were

correlated with their inputs similar to those in Table 5.2. Of these 600 inputs, the final SOM

(M5) classified 297 as fatigue crack growth, 176 as rivet fretting, and 277 as metal rubbing.

Table 5.2 AE parameters and SOM classifications.

Risetime	Counts	Energy	Duration	Amplitude	P_Counts	M5	M7	M9
25	6	0	26	41	6	crk	crk	crk
9	4	0	9	39	4	crk	**riv**	crk
3	2	0	4	36	2	crk	crk	crk
2	2	0	3	36	2	crk	crk	crk
5	3	0	6	41	2	crk	crk	crk
8	40	2	314	53	5	rub	rub	rub
6	3	0	5	37	3	crk	crk	crk
49	88	4	428	55	19	rub	rub	rub
1	2	0	3	58	1	crk	crk	crk
60	57	9	594	65	11	rub	rub	rub
11	8	0	20	45	4	crk	**rub**	crk
7	7	0	28	49	3	crk	**rub**	crk
2	62	11	376	68	6	rub	rub	rub
2	73	7	836	58	1	rub	rub	rub
2	24	2	64	64	1	riv	**rub**	riv
2	69	9	225	65	1	rub	rub	**riv**
8	4	0	10	38	4	crk	**riv**	crk
6	18	0	66	57	2	riv	**rub**	riv
19	33	1	104	47	7	riv	**rub**	riv
19	39	6	174	61	6	riv	**rub**	riv
5	54	6	429	60	1	rub	rub	rub
26	8	0	28	38	7	crk	crk	**riv**
49	62	10	186	64	15	riv	**rub**	riv
3	1	0	4	34	1	crk	crk	crk
6	6	0	382	41	2	rub	rub	rub
1	21	1	238	52	1	rub	rub	rub
5	3	0	6	40	2	crk	crk	crk
2	1	0	1	33	1	crk	crk	crk
7	4	0	9	40	3	crk	crk	crk
3	1	0	4	36	1	crk	crk	crk
61	2	0	61	35	2	riv	**crk**	riv
7	6	0	19	40	4	crk	**rub**	crk
6	3	0	5	38	2	crk	crk	crk
5	3	0	5	40	3	crk	crk	crk
1	159	7	1862	48	1	rub	rub	rub
5	2	0	5	37	2	crk	crk	crk
3	1	0	3	34	1	crk	crk	crk
1	1	0	2	32	1	crk	crk	crk
5	2	0	4	36	2	crk	crk	crk

Then the parameters were analyzed by hand. It was found that the SOM had misclassified

several of the input parameter sets. The confusion matrix in Figure 5.11 shows how the SOM

classified 24 crack signals as rivet fretting and 20 crack signals as metal rubbing. After

looking at the parameters, it was found that the LOCAN-AT data acquisition system recorded

several multiple hits during testing. Again, this is when two AE events occur almost

simultaneously, and are recorded as one event. For example, if two fatigue crack signals

occur 30 μs apart, they would be recorded as a long duration event, with the counts

parameter being the sum of the counts from each crack signal, as well as the energy

parameter. Duration would be longer. The risetime and counts-to-peak would be dependent

upon whether or not the first signal to reach the sensor was the larger of the two. The

amplitude would be that of the larger signal.

SOM M5

		C	F	R
	C	297	24	20
CLASSIFICATION	F	0	152	0
	R	0	0	257

C = Crack growth
F = Rivet fretting
R = Metal rubbing

Figure 5.11 Confusion Matrix for the Final SOM (M5)

As can be seen from the confusion matrix, the SOM did not "fail safe." In other words, when the SOM misclassified a signal, it did not classify it on the side of safety, which would result in rivet and rubbing signals being classified as crack growth signals. Instead, the SOM classified several crack signals and multiple hit signals containing cracks as rivet and rubbing signals, which would appear as though the structure was not cracking as much as it actually was. Classification accuracy: 92.7% which is comparable to the classification accuracy obtained by Almeida for his tensile lap joint specimens. Thornton did not determine classification accuracy for the waveform frequency spectrum analysis he performed on this same vessel, so no comparison can be made. Visually, it appeared that his waveform classification accuracy was somewhat better than that obtained herein using the AE parameters only.

CHAPTER 6

CONCLUSIONS AND RECOMMENDATIONS

6.1 CONCLUSIONS

- Acoustic emission nondestructive testing can be used to detect and monitor fatigue crack initiation and growth in thin 2024-T3 aluminum pressure vessels, resembling aircraft fuselages.

- A neural network, using only three AE parameters, was able to classify the three AE source mechanisms present with an accuracy of almost 93%.

- The neural network correctly classified cracking data that was collected along with data that was originally thought to be rubbing only.

- The analysis performed herein using AE parameters appears to more distinctly separate the modes of failure in the vessel than the frequency spectrum analysis from the previous research [Thornton]; however, the classification accuracy is not as good. On the other hand, AE parameter analysis requires significantly less data processing.

6.2 RECOMMENDATIONS

- Since both AE parameter analysis and waveform frequency analysis are good, but not totally conclusive, create a neural network which combines the two analysis methods. This additional information could be used to discern multiple hits from other long duration events.

- Better results may also be obtained from the addition of a parametric variable, such as strain obtained from a strain gage attached to the vessel. Most fatigue cracking is thought to occur at the point of maximum strain during a load cycle. The addition of such parametric information may help the SOM to better classify crack growth.

- Change the data acquisition system by reducing the hit lockout time (HLT) to reduce the number of multiple hits [Kouvarakos and Hill]. Since the duration for crack signals are very short, a long HLT is not required.

- Since only one of the 2024-T3 vessels was used herein, a network could be created using data from all five vessels. This would introduce 7075-T6 aluminum into the training set, which would, in turn, result in a more generic network that could be applied to more than one structure and more than one material.

- A final step would be to program a generic neural network onto a computer chip to be included in an in-flight fatigue crack detection system for aircraft. Ideally, a single neural network could be used for different aircraft structures with different materials. A prototype system is currently being designed to provide aircraft with a real time in-flight fatigue crack growth monitoring capability.

REFERENCES

1. O'Lone, R. G., "Safety of Aging Aircraft Undergoes Reassessment," Aviation Week and Space Technology, Vol. 128, Issue 20, May 16, 1988, pp. 16-18.

2. Parrish, Budd S., "An In-Flight Acoustic Crack Detection System (ACDS) for the C/KC-135 Aircraft," Presented at the National Fall Conference of the American Society for Nondestructive Testing, Columbus, Ohio, October 1979, pp. 33-35.

3. McBride, S. L. and Maclachlan, J. W., "In-Flight Acoustic Emission Monitoring of a Wing Attachment Component," Journal of Acoustic Emission, Vol. 1, Number 4, pp. 223-228.

4. Scala, C. M. and Coyle, R. A., "Acoustic Emission Waveform Analysis to Identify Fatigue Crack Propagation in a Mirage Aircraft," Journal of Acoustic Emission, Vol. 6, Number 4, pp. 249-256.

5. Scala, C. M., McCardle, J. F., and Bowles, S. J., "Acoustic Emission Monitoring of a Fatigue Test of an F/A-18 Bulkhead," Journal of Acoustic Emission, Vol. 10, Number 3/4, pp. 49-60.

6. Almeida, A. F. and Hill, E. v. K., "Neural Network Detection of Fatigue Crack Growth in Riveted Joints Using Acoustic Emission." Materials Evaluation, Vol. 53, Number 1, 1995, pp. 76-82.

7. Ely, T. M. and Hill, E. v. K., "Neural Network Classification of Acoustic Emission Data from Graphite/Epoxy Tensile Test Specimen," ASNT 1995 Spring Conference, American Society for Nondestructive Testing, Columbus, OH, 1995, pp. 109-111.

8. Thornton, W. P., "Classification of Acoustic Emission Signals from an Aluminum Pressure Vessel Using a Self-Organizing Map," M.S. Thesis, Embry-Riddle Aeronautical University, Daytona Beach, FL, 1995.

9. Walker, J. L. and Hill, E. v. K., "An Introduction to Neural Networks: A Tutorial," presented at the First International Conference On Nonlinear Problems in Aviation and Aerospace, Daytona Beach, FL, May 1996.

10. Walker, J. L., Workman, G. L., Russel, S. S., and Hill, E. v. K., "Neural Network Burst Prediction in Impact Damaged Kevlar/Epoxy Bottles from Acoustic Emission Amplitude Data," presented at the First International Conference On Nonlinear Problems in Aviation and Aerospace, Daytona Beach, FL, May 1996.

11. Fausett, L., Fundamentals of Neural Networks: Architecture, Algorithms, and Applications, Prentice Hall, Englewood Cliffs, NJ, 1994, pp. 170-175.

12.   Kouvarakos, M., and Hill, Eric, v. K., "Isolating Failure Mechanisms in Fiberglass Epoxy from Acoustic Emission Signal Parameters," <u>Materials Evaluation</u>, vol. 54, Number 9, pp. 1025-1031.

BIBLIOGRAPHY

1.   Fausett, L., <u>Fundamentals of Neural Networks: Architecture, Algorithms, and Applications,</u> (Englewood Cliffs, NJ, 1994).

2.   Miller, R. K. and McIntire, P., <u>Acoustic Emission Testing,</u> Volume 5 of <u>Nondestructive Testing Handbook,</u> second edition (Columbus, OH: American Society for Nondestructive Testing, 1987).